International Geology Review
Publication details, including instructions for authors and subscription information:
http://www.tandfonline.com/loi/tigr20

The Mazarrón basin, SE Spain: a study of mineralization processes, evolving magmatic series, and geothermal activity

E. Crespo[a], J. Lillo[bce], R. Oyarzun[ac], P. Cubas[cd] & M. Leal[e]

[a] Departamento de Cristalografía y Mineralogía, Facultad de Ciencias Geológicas, Universidad Complutense, 28040, Madrid, Spain

[b] Escuela Superior de Ciencias Experimentales y Tecnología, Universidad Rey Juan Carlos, Tulipán s/n, 28933, Móstoles, Madrid, Spain

[c] Instituto de Geología Aplicada, E.I.M.I. Almadén, Universidad de Castilla-La Mancha, Plaza Manuel Meca 1, 13400, Almadén, (Ciudad Real), Spain

[d] Departamento de Biología Vegetal II, Facultad de Farmacia, Universidad Complutense, 28040, Madrid, Spain

[e] Instituto IMDEA Agua, Punto Net 4, 28805, Alcalá de Henares, Spain

Published online: 21 Jun 2013.

To cite this article: E. Crespo, J. Lillo, R. Oyarzun, P. Cubas & M. Leal (2013) The Mazarrón basin, SE Spain: a study of mineralization processes, evolving magmatic series, and geothermal activity, International Geology Review, 55:16, 1978-1990, DOI: 10.1080/00206814.2013.810379

To link to this article: http://dx.doi.org/10.1080/00206814.2013.810379

International Geology Review, 2013
Vol. 55, No. 16, 1978–1990, http://dx.doi.org/10.1080/00206814.2013.810379

Taylor & Francis
Taylor & Francis Group

The Mazarrón basin, SE Spain: a study of mineralization processes, evolving magmatic series, and geothermal activity

E. Crespo[a], J. Lillo[b,c,e], R. Oyarzun[a,c]*, P. Cubas[c,d] and M. Leal[e]

[a]*Departamento de Cristalografía y Mineralogía, Facultad de Ciencias Geológicas, Universidad Complutense, 28040 Madrid, Spain;* [b]*Escuela Superior de Ciencias Experimentales y Tecnología, Universidad Rey Juan Carlos, Tulipán s/n, 28933 Móstoles, Madrid, Spain;* [c]*Instituto de Geología Aplicada, E.I.M.I. Almadén, Universidad de Castilla-La Mancha, Plaza Manuel Meca 1, 13400 Almadén, (Ciudad Real), Spain;* [d]*Departamento de Biología Vegetal II, Facultad de Farmacia, Universidad Complutense, 28040 Madrid, Spain;* [e]*Instituto IMDEA Agua, Punto Net 4, 28805 Alcalá de Henares, Spain*

(*Accepted 24 May 2013*)

The Miocene to Present Mazarrón basin provides a window on the metallogenic role of an evolving magmatic series. High-K calc–alkaline magmas gave rise to an important cluster of Pb–Zn–Ag–Cu vein and stockwork deposits emplaced in dacitic to rhyodacitic domes, part of a complex volcanic–metallogenic province (Au, Hg, Pb–Zn–Cu–Ag, Sn) stretching for ∼150 km along the Mediterranean coast of SE Spain. By Pliocene time the former magmatic series had been replaced by intraplate alkaline basaltic volcanism, thus becoming the southern branch of the Western/Central Europe alkaline province. In terms of base metal sulphide deposits, this European province is barren, although it triggered widespread, CO_2-rich geothermal activity. Modern geothermal activity at El Saladillo (Mazarrón) resulted in the deposition of carbonate sinter deposits and formation of microbial mats. Proximal facies consist of millimetric to centimetric multicoloured layers of microbial mats, including yellow-orange thin bands of calcified bacteria and mineral growths of aragonite and calcite; green layers of live thermophilic *Lyngbya*-type cyanobacteria; black, degraded organic matter; and pyrite as the sole sulphide phase. Except for arsenic (37–63 μg g^{-1}), all of the studied trace elements (Ag, Ba, Bi, Cd, Cu, Pb, Sb, Se, and Sn) appear in remarkably low concentrations in the geothermal sinters. This is consistent with compositional data for the El Saladillo waters, with no significant metal concentrations. We present the first conceptual model (Miocene to Present) for the ore-forming processes, magmatism, CO_2 degasification, and geothermal activity for this realm. We argue that the time- and space-limited character of this volcanism (small, scattered outcrops), the deep magma emplacement level, the metal sulphide behaviour in alkaline basaltic magmatic chambers, and the dry character of these magmas prevented any metallogenic interaction between the chambers and the much shallower meteoric waters that drove the El Saladillo geothermal system and others of the same kind in Spain and elsewhere in Europe.

Keywords: Mazarrón basin; SE Spain; base metal deposits; high-K calc–alkaline aqueous fluids; barren intraplate alkaline magmatism; CO_2 degasification; geothermal activity

Introduction

The drilling of a 535 m deep well in the northern realm of the Mazarrón Basin (SE Spain) (Figures 1(A) and 1(B)) in 1985 led to the discovery of CO_2-rich geothermal waters (46–48°C) at the El Saladillo site (Pérez del Villar Guillén *et al.* 2008) (Figures 1 and 2(A) and 2(B)). This can be regarded as the 'barren culmination' of long-lasting hydrothermal activity in this Spanish realm, which first led to the formation of Pb–Zn–Ag–Cu vein and stockwork deposits in Miocene time (Mazarrón District) (Figure 1(B)). When we started this research the initial idea was that the El Saladillo geothermal waters could have either induced leaching, transport, and deposition of base metals or remobilization of hidden base metal deposits (such as those from the southern realm of the basin) (Figure 1(B)). However, the geochemical results for the carbonate sinters indicated concentrations lower than those of the country rocks. Although we knew that the late, intraplate basaltic alkaline volcanism had not triggered formation of sulphide metal deposits in the basaltic alkaline European province, we lacked a comprehensive explanation on why this was the case. After all, these magmas have enough sulphur and indeed trigger hydrothermal activity (e.g. Kovalenko *et al.* 2007). Thus, to search for plausible answers we concentrated our efforts on the Pliocene to present alkaline magmatism and related geothermal activity from Spain.

Geological and geophysical studies indicate that SE Spain (and elsewhere in the peninsula) is characterized by an important deep thermal anomaly and persistent

*Corresponding author. Email: oyarzun@ucm.es

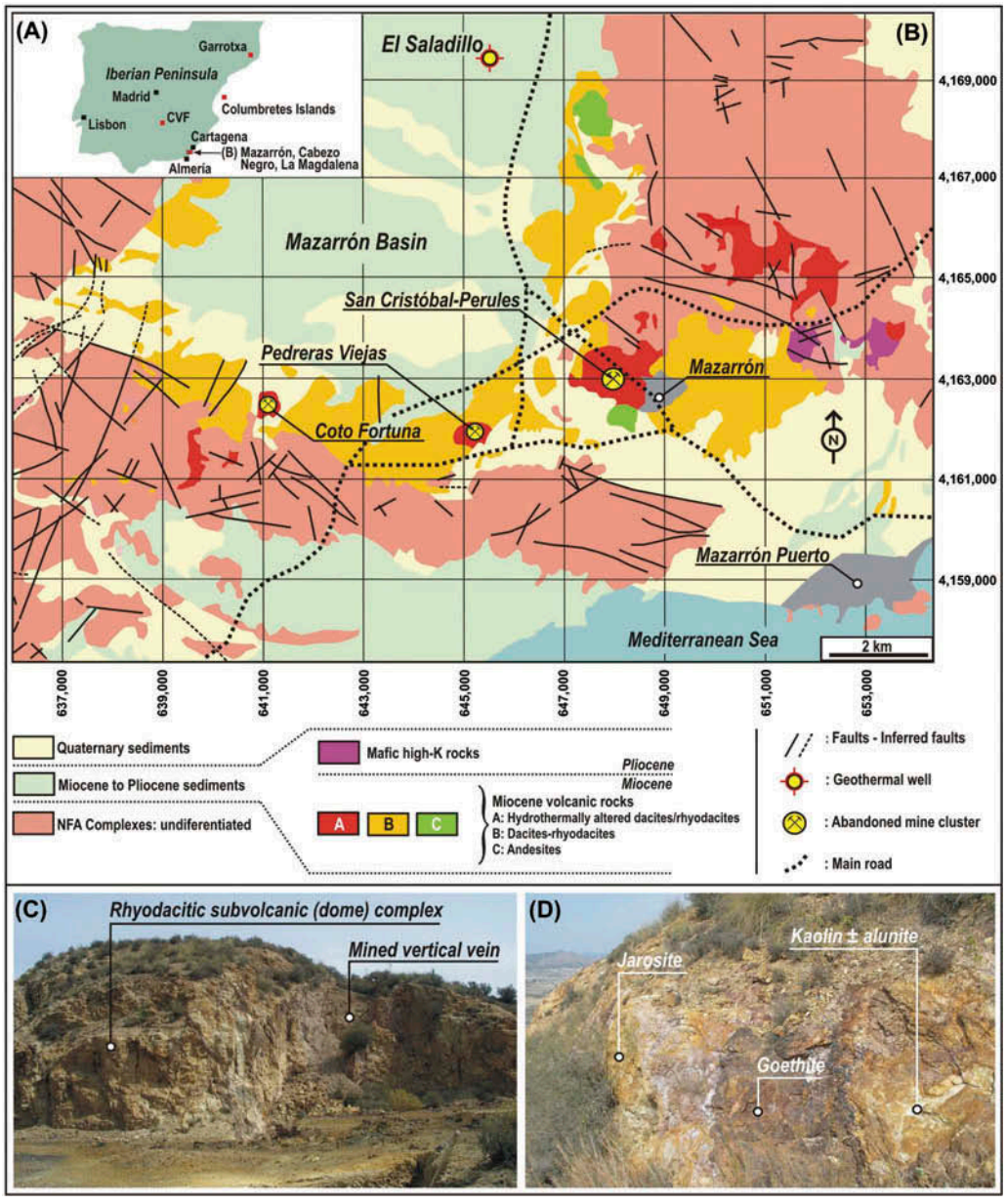

Figure 1. The Mazarrón Basin. (A) Location map, also depicting localities with extruded alkali basalts (solid red squares) mentioned in the text; CVF, Calatrava Volcanic Field. (B) Geology of Mazarrón (modified after Oyarzun *et al*. 2011). NFA, Nevado Filábrides and Alpujárrides metamorphic complexes (graphitic black schists, feldespathic schists, quartzites, marbles). (C) Aspect of the volcanic domes at San Cristóbal–Perules, also depicting a mined subvertical (leached) thick vein. (D) A complex structural array of leached veins at San Cristóbal–Perules.

magmatism that have lasted from Miocene to Quaternary time (Figure 1(A)), whereas isotopic studies on the thermal waters indicate a deep origin for CO_2. The Mazarrón basin hosts Miocene to Pliocene marine sediments and volcanic rocks overlying a basement characterized by Alpine metamorphic complexes (Figure 1(B)). From a metallogenic point of view, the basin is well known because of the presence of the historical Mazarrón Mining District (Pb–Zn–Ag–Cu; San Cristóbal – Perules, Pedreras Viejas, and Coto Fortuna), which is genetically related to the emplacement of Miocene dacitic domes (Oyarzun *et al.* 2011) (Figure 1(B)). We briefly review the geology and hydrology of this realm and present mineralogical and geochemical evidence regarding the geothermal carbonate sinter deposits of El Saladillo, including the first description for this site of biomineralization processes. Last but not least, we also present the first integrated model for this realm, putting together all of the major geologic features that played a part in the building up of magmatism and hydrothermal activity from Miocene to Present time.

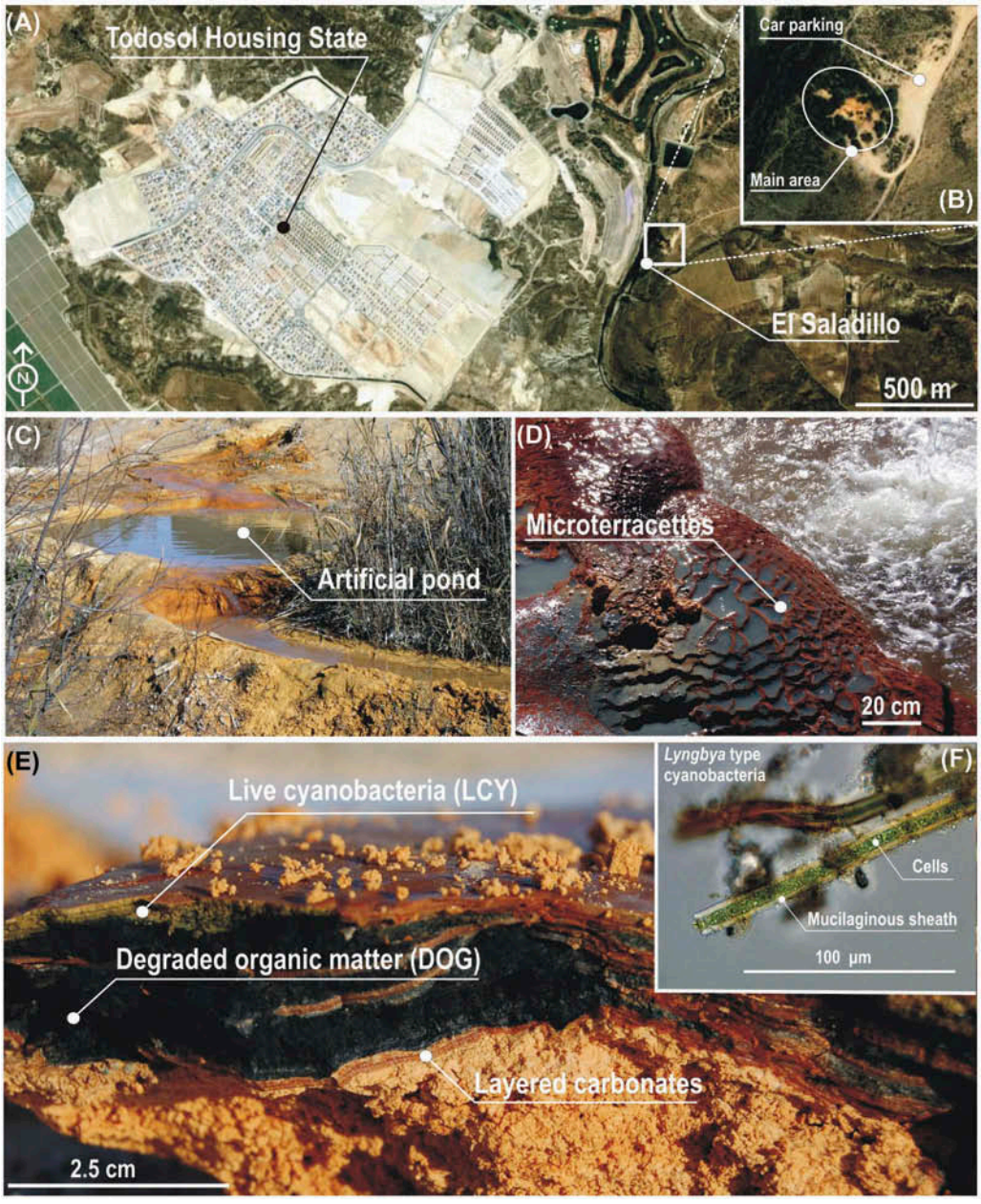

Figure 2. The El Saladillo site and facies. (A) Location of El Saladillo site (image: Google Earth). (B) Closer view of El Saladillo site (image: Google Earth). (C) Ponds of thermal waters and carbonate sinters. (D) Proximal facies with bright-coloured microterracettes. (E) Banding in proximal facies; the *black* layers correspond to degraded microbial mats. (F) *Lyngbya*-type cyanobacteria from El Saladillo.

Geology

Regional and local setting including the Pb–Zn–Ag–Cu deposits

The geology of SE Spain (Almería and Murcia regions) is characterized by the ubiquitous presence of the two largest Alpine complexes in the Iberian Peninsula: Alpujárrides and Nevado-Filábrides. These units were intensively folded and thrusted during the late Oligocene–early Miocene, and later underwent extensional collapse through major detachment systems in middle–late Miocene time (Doblas and Oyarzun 1989). This episode was accompanied by important calc–alkaline to high-K calc–alkaline volcanism (andesites, dacites, and rhyolites) along the Almería–Cartagena Volcanic Belt (Figure 1(A)), whereas sedimentation took place within restricted marine sedimentary basins such as that of Mazarrón (Doblas and Oyarzun 1989). The volcanism triggered hydrothermal activity that led to the formation of important clusters of ore deposits such as those of Au at Rodalquilar (Almería) and Pb–Zn–(Ag) at Mazarrón and La Unión (Murcia) (Oyarzun *et al.* 1995).

The volcanic activity had a second pulse during Pliocene time when basaltic alkaline rocks were extruded forming small outcrops and vents, such as those of Cabezo Negro–La Magdalena (e.g. Cebriá *et al.* 2009) about 20 km eastward from Mazarrón (Figure 1(A)). This pulse has been interpreted as a volcanic episode similar to the contemporaneous alkaline basaltic volcanism of the Iberian Peninsula and Western/Central Europe (Wilson and Downes 2006; Cebriá *et al.* 2009). This volcanism has been persistent in Spain, lasting until Quaternary time, with some very young ages between 13,160 and 15,710 years BP at Garrotxa (Puiguriguer *et al.* 2012) (Figure 1(A)). On the other hand, Miocene and Pliocene marine sedimentation in the Betics realm developed in Neogene basins, whereas the Mazarrón trough was infilled during Tortonian-Messinian and Pliocene time by marine sediments comprising marls, limestones, sandstones, and conglomerates. Coeval volcanic activity gave rise to high-K calc–alkaline andesites, dacites, and rhyodacites that were emplaced as domes and lavas (Figure 1(C)). The southern realm of the volcanic rim hosts Pb–Zn–Ag–Cu deposits of the vein and stockwork type (Figures 1(C) and (D)), whereas the main ore deposits clusters are (from west to east) Coto Fortuna, Pedreras Viejas, and San Cristóbal-Perules (Figure 1(B)). These clusters are characterized by the presence of dacitic to rhyodacitic domes that underwent strong and pervasive advanced argillic alteration, with kaolinite, alunite, and silica formation (Figure 1(D)). Main ore minerals are pyrite, sphalerite, and Ag-bearing galena, whereas other sulphides include chalcopyrite, tetrahedrite–tennantite, arsenopyrite, cinnabar, stibnite, and berthierite (Rodríguez and Hidalgo 1997; Oyarzun *et al.* 2011). The district was first mined for lead in Roman time, later for the alum (aluminium sulphate: alunite) during the fifteenth to sixteenth centuries, then for the alum wastes from 1774 to 1953, and finally for lead, silver, and zinc during the nineteenth to twentieth centuries (until the early 1960s) (Rodríguez and Hidalgo 1997).

Regional geothermal activity and the El Saladillo site

SE Spain is characterized by the existence of modern CO_2-rich geothermal systems, which appear to be related to currently tectonically active fault systems (Cerón *et al.* 1998, 2000a). Regional geophysical studies indicate that a low-velocity zone pervades the uppermost mantle and that the overlying crust has a high Vp/Vs ratio and a prominent intracrustal low-velocity zone (Julià *et al.* 2005). These authors suggest that the observations may result from rapidly ascending magma diapirs ponding at intracrustal levels. In this respect, Cebriá *et al*. (2009) indicate that the basaltic alkaline magmas would have formed through the interaction between primitive melts generated from a sublithospheric mantle source and liquids derived from the overlying lithospheric mantle. This, together with the existence of crustal-scale fault zones, may well explain the thermal anomalies, geothermal activity, and a deep source for CO_2 (Cerón *et al.* 1998).

The El Saladillo geothermal system (Figures 1(B) and 2(A)–2(F)) has been probed up to 535 m deep and is hosted by Miocene sediments and volcanic rocks of the Mazarrón basin and metamorphic rocks of the Nevado-Filábrides Complex. The bubbling gas consists mainly of CO_2 (70–90%) and traces of CH_4, N_2, and He, and the waters are relatively reducing with an Eh of about −54 mV, slightly acidic with a pH around 6.6 and with temperatures ranging between 46°C and 47.8°C (Pérez del Villar Guillén *et al.* 2008). The El Saladillo geothermal system is included in the so-called Alto del Reventón Geothermal Unit, which is characterized by the presence of a deep saline CO_2-rich aquifer and is related to the aforementioned regional geothermal anomaly in SE Spain. The aquifer corresponds to a Nevado-Filábrides unit composed of feldespathic schists, quartzites, and marbles that form the substrate of the Miocene sedimentary basin and is sealed by the overlaying Miocene marly units. Based on chemical geothermometers, the temperature of groundwater sources has been estimated to be 70–96°C (Cerón *et al.* 2000a). The regional geothermal anomaly affects aquifers with groundwaters characterized by high bicarbonate concentrations, high pCO_2, and relatively high electrical conductivity (Cerón *et al.* 1998, 2000a).

The El Saladillo carbon isotopic data with $\delta^{13}C_{CO2(gas)}$ values (relative to the V-PDB standard) ranging from −9.7‰ to −12.6‰ and $\delta^{13}C_{\text{dissolved inorganic carbon}}$ ranging from −5.4 to −5.8‰ (Pérez del Villar Guillén *et al.* 2008) are consistent with the regional data from Cerón *et al*. (2000a), who propose that significant amounts of CO_2 were derived from deep sources, either mantle and/or by processes of thermometamorphism of carbonate rocks. Besides, $\delta^{18}O_{\text{dissolved sulphate}}$ in El Saladillo water is in the range of +12.7‰ to +17.8‰ (V-SMOW Standard), which is interpreted by Pérez del Villar Guillén *et al*. (2008) as indicative of the presence of hydrothermal sulphates. On the other hand, $\delta^{34}S_{\text{dissolved sulphate}}$ values of +17.6‰ (CDT Standard) are in the $\delta^{34}S$ range of evaporitic gypsum in Messinian sedimentary units in the region (Pérez del Villar Guillén *et al.* 2008). On the basis of $\delta^{18}O$ and δD regional data, Cerón *et al*. (1998) suggested the occurrence of mixing processes between meteoric waters (involving washing of evaporitic rocks; Cerón *et al.* 2000b) and deep hot waters.

Sampling and analytical procedures

We took samples of the geothermal sinters and host rocks with the aid of a portable sampling drill machine for core extraction and later geochemical and mineralogical studies; however, samples destined for detailed mineralogical and biological studies were carefully obtained with chisel and hammer. We also took water samples directly from

the source. We concentrated the sampling on the carbonate sinters (microbial mats), although baseline samples were also taken from Miocene marls in the vicinity. The samples were stored in plastic bags (sinters, soils) and bottles (water); the solid samples were crushed and sieved at the Department of Biology and Geology laboratory facilities (Rey Juan Carlos University: URJC; Móstoles-Madrid), and part of the material was sent to Activation Laboratories Ltd. (Actlabs; Canada) to be analysed by TD (total digestion) ICP-MS (inductively coupled plasma mass spectrometry). Quality control at the Actlabs Laboratories is done by analysing duplicate samples and blanks to check precision, whereas accuracy is obtained by using certified standards (GXR series). The mineralogy and mineral chemistry of samples were studied by XRD (instrument: Philips, model PW3040/00 X'Pert MPD/MRD) and FEG-SEM-EDX (instrument: Nova Nano SEM230, scanning electron microscope (SEM) and ESEM) at the CAT facilities of the URJC. For the observation of cyanobacteria, small pieces of material were separated from the rock, disaggregated in distilled water, and coarse material was discarded by a short centrifugation. The remaining liquid was transferred to sterile tubes, mounted in slides, and observed under a Nikon Eclipse 80i microscope. The water samples collected from the pipe outlet were refrigerated for conservation before the analyses. Major ions in water samples were analysed by ion chromatography (metrohm ion chromatography advanced compact IC with two-channel) according to the Standard Methods for the Examination of Water and Wastewater (APHA *et al*. 2005) at the IMDEA Water Institute (Madrid). Metals and metalloids of water samples were analysed by ICP-MS at Actlabs and also at the IMDEA laboratories. Quality control is accomplished by analysing duplicate samples and blanks to check precision, whereas accuracy is obtained by using certified standards (NIST 1643e and SLRS-5). Geochemical modelling of water data was performed with the PHREEQC code (Parkhurst and Appelo 1999) and with a revised version of the Liquid_Analysis_v3-Powell-2010-Stanford GW spreadsheet (Powell and Cumming 2010).

Table 1. Compositional data for water samples from El Saladillo well (samples SA).

	SA-1	SA-2
pH	6.6	6.7
T (°C)	46	47
EC (µS/cm)	10,590.00	10,440.00
Eh (mV)	−52.00	−56.00
Cl^- (mg/l)	1265.30	1241.50
SO_4^{2-} (mg/l)	3565.40	3604.60
HCO_3^- (mg/l)	1164.60	885.60
Li^+ (mg/l)	2.84	3.03
Na^+ (mg/l)	2040.20	2064.80
K^+ (mg/l)	85.50	86.90
Mg^{2+} (mg/l)	235.70	237.60
Ca^{2+} (mg/l)	313.90	228.60
Fe (mg/l)	3.53	3.96
Si (mg/l)	18.00	18.90
Sr (mg/l)	8.83	8.10
Al (mg/l)	10.00	9.00
As (µg/l)	34.90	34.30
Ba (µg/l)	3.40	2.00
Cd (µg/l)	0.02	0.02
Ce (µg/l)	0.01	0.01
Cs (µg/l)	197.00	194.00
Cu (µg/l)	21.00	22.40
Er (µg/l)	0.002	0.002
Hg (µg/l)	0.70	<0.40
Ho (µg/l)	0.004	0.004
La (µg/l)	0.006	0.008
Mn (µg/l)	0.90	1.30
Mo (µg/l)	0.90	1.00
Ni (µg/l)	10.30	10.30
Pb (µg/l)	0.10	0.13
Rb (µg/l)	351.00	355.00
Sb (µg/l)	0.20	0.22
Sc (µg/l)	6.00	6.00
Se (µg/l)	12.70	9.40
Th (µg/l)	0.05	0.02
Ti (µg/l)	5.60	6.00
U (µg/l)	3.58	3.41
Y (µg/l)	0.07	0.06
Zn (µg/l)	7.00	6.40
Zr (µg/l)	0.06	0.06

Note: EC, electrical conductivity.

Results and discussion

The El Saladillo site: sinter facies and geochemistry

Published chemical and isotopic data for the thermal waters of the El Saladillo suggested that the system had remained almost constant since the well was drilled in 1985 (Pérez del Villar Guillén *et al.* 2008). However, data obtained in this work indicate some significant variations regarding the major ionic species (HCO_3^-, SO_4^{2-}), and Ca^{2+} and Mg^{2+} ratios have occurred (Table 1). The analysed water is of the sodium sulphate type, with anion and cation trends being $rSO_4^{2-} > rCl^- > rHCO_3^-$ and $rNa^+ > rMg^{2+} > rCa^{2+}$. This suggests that water has evolved to a slightly richer composition in chloride and magnesium since 1985. Geochemical modelling suggests saturation or near-saturation in haematite, dolomite, goethite, gibbsite, calcite, strontianite, aragonite, some Pb, Cu, and Zn selenide minerals, magnesite, gypsum, and baryte.

Where the water emerges from the pipe and touches the ground surface (Figures 2(C)) and 2(D)), 5–10 cm-wide orange-coloured microterracettes (*sensu* Fouke *et al.* 2000) have formed; they are hard to break and form proximal facies (Figure 2D). These are decimetric-thick layered structures with millimetric to centrimetric bands of (Figure 2(E)) (1) carbonate (aragonite-calcite); (2) green-coloured live colonies of thermophilic cyanobacteria (*Lyngbya* type; e.g. Lukavský *et al.* 2011) (Figure 2F); and (3) degraded organic matter with a characteristic black

Table 2. Trace element chemistry of the El Saladillo carbonate sinters, Miocene marls, and carbonate-rich stream sediments from a nearby seasonal river (Oyarzun *et al*. 2011).

Element (μg g^{-1})	Ag	As	Ba	Bi	Cd	Cu	Pb	Sb	Se	Sn	Te	Zn
Sample						El Saladillo carbonate sinters						
S-1B	0.1	62.6	39	0.04	<0.1	2.2	37.5	0.8	0.3	<1	<0.1	16.3
S-1AC	<0.05	37.2	26	<0.02	<0.1	1.5	4.7	0.7	0.4	<1	0.2	9.6
S-1AO	<0.05	30.4	33	<0.02	<0.1	1.8	9.2	<0.2	<0.1	<1	<0.1	17.0
SA-1(T)	3.30	34.5	28	0.08	<0.1	3.2	20.0	0.3	<0.1	<1	<0.1	17.3
SA-2(T)	0.52	48.2	21	0.04	<0.1	1.1	1.9	<0.2	0.3	<1	0.2	9.7
SA-3(T)	0.27	37.9	18	0.03	<0.1	1.4	8.1	<0.2	<0.1	<1	0.3	6.6
						El Saladillo Miocene marls						
SA-4	0.07	7.9	301	0.18	0.2	16.7	17.1	0.7	0.8	2	<0.1	44.4
SA-5	0.88	7.3	299	0.21	<0.1	21.2	14.2	1.1	0.3	3	<0.1	46.9
						Mazarrón stream sediments (Rambla de las Moreras)						
RS-01	0.14	15.4	313	<0.02	0.2	19.7	79.5	1.2	0.6	3	<0.1	72.9
RS-02	0.23	15.6	231	<0.02	0.3	15	62.7	1.4	2.4	3	<0.1	59.8

Note: S-1B, S-1AC, and S-1AO: proximal facies; SA-1(T), SA-2(T), and SA-3(T): distal facies.

colour. In this respect, the presence of microbial mats of *Lyngbya* in travertine crusts creates favourable microniches for photosynthetically induced calcification (e.g. Pentecost 1995). Distal facies (a few metres down slope) are characterized by a softer, powdery material that keeps nevertheless equivalent mineralogical and geochemical (Table 2) characteristics to those of the proximal facies. The trace elements chosen for this study are relevant to the metallogenic signature of the basin, dominated by the Mazarrón Pb–Zn–Ag–Cu ore deposits (Figure 1(B)) (Oyarzun *et al.* 2011). However, with the sole exception of arsenic, the carbonate sinters have very low concentrations of metals (Table 2), which is consistent with the compositional data for the well's water (Table 1). In this regard, the geochemical behaviour of arsenic in natural waters departs from that of other cations. Although this element is mobile under a wide range of pH and Eh as either oxyanions of arsenite (As^{3+}) or arsenate (As^{5+}) (Smedley and Kinniburgh 2002), in oxic environments arsenic tends to be sorbed as As^{5+} (either by adsorption or coprecipitation) in Fe-oxides, hydroxides, and oxyhydroxides (Bowell 1994) and carbonate minerals, such as calcite (Alexandratos *et al.* 2007).

Carbonates, sulphides, and bacteria

Carbonate spring deposits form through the interplay of biotic and abiotic processes (Rainey and Jones 2009). These complex systems result in the formation of carbonate sinter deposits, which in turn are made of microbial (algal) mats, that is, layered structures formed by filamentous algae like cyanobacteria among many others. However, a key question here is how the metabolic activity of cyanobacteria can lead biomineralization, in this case to precipitation of carbonates and sulphides. Another question relates to how can all this happen within a superficial, highly oxygenated environment. It all begins with the most basic organic reaction in nature, the photosynthesis by cyanobacteria (Baumgartner *et al.* 2006), as it have been happening since Archaean time (e.g. Oyarzun *et al.* 2008). Photosynthetic processes driven by cyanobacteria primarily lead to (Baumgartner *et al.* 2006):

$$CO_2 + H_2O \rightarrow CH_2O + O_2.$$

However, if sufficient calcium and sulphate is present in the solution (Table 1), the microbial metabolism results in an increase in alkalinity which moves the equilibrium towards calcium carbonate precipitation, which can be summarized as (Baumgartner *et al.* 2006):

$$SO_4^{2-} + 2CH_2O + OH^- + Ca^{2+} \rightarrow CaCO_3 + CO_2 + 2H_2O + HS^-.$$

Thus, key aspects of carbonate biomineralization are, on the one hand, the 'alkalinity engine' and, on the other hand, the organic matrix comprised extracellular polymeric substances which may provide a 'template' for carbonate nucleation (Dupraz *et al.* 2009). In this regard, the latter chemical reaction not only explains the precipitation of calcium carbonate but also indicates the formation of HS^- via reduction of SO_4^{2-}; all this providing that the sulphate anion is present in the solution as it happens to be the case at El Saladillo. In turn, formation of HS^- plays a key role in the biomineralization process because if Fe^{3+} is also available it follows that (Wei and Osseo-Asare 1996):

$$2Fe^{3+} + HS^- \rightarrow 2Fe^{2+} + S^0 + H^+$$

$$Fe^{2+} + HS^- \rightarrow FeS + H^+$$

$$FeS + S^0 \rightarrow FeS_2.$$

Alternatively, pyrite formation at El Saladillo could be related to sulphate-reducing bacteria (SRB), which are very small organisms in the range of 0.5–1.3 × 0.8–5 μm (e.g. *Desulfovibrio*) and 0.5–2 × 2–9 μm (e.g. *Desulfotomaculum*), with cell forms including cocci, rods, curved types, cell aggregates, and multicellular gliding filaments (Wargin *et al.* 2007). Although their presence in oxygenated microenvironments was initially thought to be related to the use of survival strategies (day/night cycles) to escape oxygen stress in cyanobacterial mats (e.g. Krekeler *et al.* 1998), a few years ago their behaviour in oxygenated environments began to be fully understood. In this respect, it is now accepted that SRB can actually tolerate (Wargin *et al.* 2007) and even breathe oxygen to the point in which they can be abundant and active in oxygenated zones of microbial mats (Baumgartner *et al.* 2006). In this respect, apart from *Lyngbya*-type cyanobacteria, we found other, smaller rod-shaped and curved forms that could possibly represent SRB because of their small size and ecological niche (Figures 3(A)–3(C)) (e.g. Wargin *et al.* 2007). Unfortunately, these forms are too small for a proper identification by conventional microscopy and the use of molecular markers is beyond the scope and possibilities of this work.

Pyrite at El Saladillo sinters appears in two different textures, octahedral crystals and framboids (Figures 3(C)–3(F)). Octahedral pyrite occurs as loose homogeneous masses covering aggregates of calcite and aragonite crystals (Figures 3(D) and 3(E)). These crystals display two different features: (1) very well-developed octahedral morphologies with a very uniform size of approximately 2 μm (Figure 3(D)) and (2) more rounded shapes of smaller size (approximately 1.5 μm) (Figure 3(E)). The octahedral crystals show smooth faces with no bacterial rods on their surface, whereas the framboids are not abundant and occur as sets of several sub-spherical to spherical aggregates of minute pyrite crystals (Figure 3(C)). The microcrystals that form the individual framboids are equidimensional cubes of pyrite and range from approximately 0.3 to 1 μm in size. Though no two-dimensional sections were observed and precise differentiation between ordered and disordered internal microcrystalline structure could not be performed (e.g. Ohfuji and Rickard 2005), it seems nevertheless that the microcrystals are packed sharing a common orientation, therefore they could be classified as ordered framboidal pyrites (Butler and Rickard 2000). Almost all the spheroidal pyrite aggregates observed in the studied samples can be classified as framboidal because all of them are spheroidal clusters of equidimensional and equimorphic microcrystals (Ohfuji and Rickard 2005). Nevertheless, it seems that smaller framboids (Figure 3(F)) are not uniform and present a less ordered microstructure compared to the larger counterparts. Moreover, microcrystals in such framboids (approximately 0.3 μm) display a certain degree of heterogeneity, sub-euhedral textures are similar to ovoidal morphologies; therefore, they cannot be regarded as framboidal pyrites.

On the other hand, it is a widely held view at present that formation of framboidal pyrite is induced by inorganic processes (e.g. Ohfuji and Rickard 2005), although the process could not operate without the activity of SRB as source of sulphur (see reactions given earlier). Besides, the clusters of octahedral pyrite crystals (Figure 3(D)) are well developed without any microbial features on their surface; therefore, an inorganic origin is here suggested, which stresses the hybrid biotic–abiotic character of mineral formation in these microenvironments (e.g. Rainey and Jones 2009). Additionally, the presence of smaller and rather 'rounded' octahedral pyrite crystals (Figure 3(E)) suggests an intermediate step between the framboids and the aggregates of larger and well-developed octahedral crystals. Since octahedral pyrite seems to be produced by secondary growth from the framboids, this pyrite is related to microbial activity.

The alkaline basaltic volcanism: some final considerations

We have left for the final part of the discussion the role of alkaline basaltic volcanism in the generation of CO_2-rich fluids and the availability/unavailability of metals. In this regard, the Calatrava Volcanic Field (CVF) (Figure 1(A)) may provide a key site for the understanding of the Pliocene to present geothermal activity in Spain in more than one sense. First, this is a CO_2-rich volcanism that gave rise to foidites, melilitites, and carbonatites that can be regarded as an ultra-alkaline rock association (Stoppa *et al.* 2012). The CVF is well known by its numerous volcanic landforms and the so-called 'hervideros', a Spanish word meaning 'boiling spots'. This can be a misleading term that does not necessarily imply high T but water effervescence due to the massive release of CO_2 (Crespo *et al.* 1995). The most famous recent hervidero was that of Bolaños de Calatrava, which according to Stoppa *et al*. (2012) flooded an area of ~90,000 m^2 in 2012 and vented up to 40 tonnes of CO_2/day. This violent water jet had a gaseous composition of about 90% vol. of CO_2, whereas an estimation of P-T conditions for the deep-seated hydrothermal system are about 118°C and 63 bar (Stoppa *et al.* 2012).

One may argue that the isotopic evidence for a deep-seated, mantle origin of carbon is not entirely convincing for the southern Miocene basins of Spain; however, similar phenomena are also observed in southern central Spain at Calatrava (Figure 1(A)). These two tectonic realms are different in more than a way, but they have a key element in common: both host the same CO_2-rich alkaline basaltic intraplate volcanism (e.g. Bailey and Kearns 2012). In this regard, while the isotopic data for carbon can be subjected to alternative (and valid) interpretations, the mineralogical evidence should settle things up. For

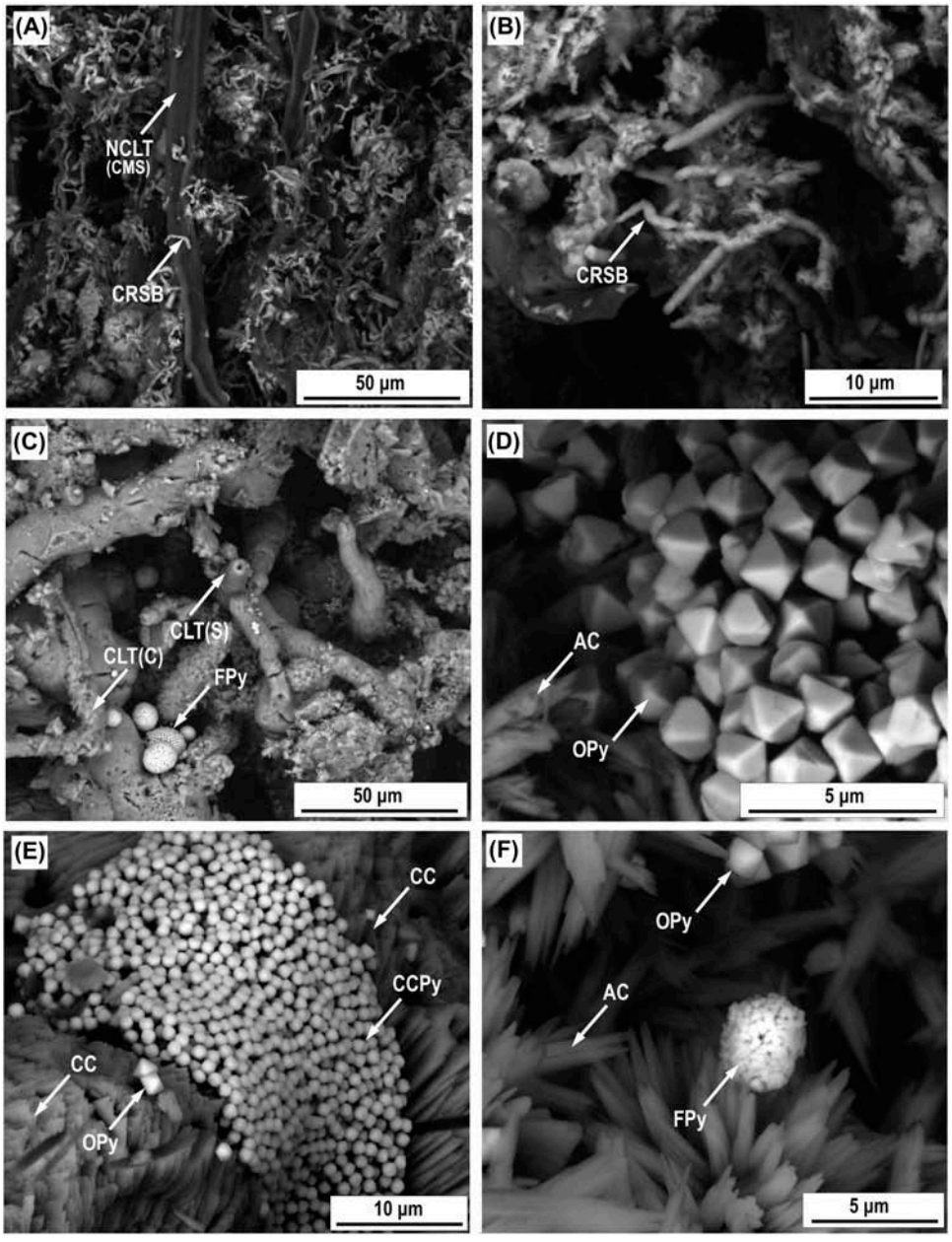

Figure 3. SEM images of bacteria, and carbonate and sulphide mineral phases. (A) Large non-calcified *Lyngbya*-type cyanobacteria (NCLT) with collapsed mucilaginous sheath (CMS) (see also Figure 2F), and much smaller curved rod-shaped bacteria (CRSB). (B) Detailed view of the combined curved rod-shaped bacterial forms (CRSB) that could represent sulphate-reducing bacteria. (C) Smoothly (S) and coarsely (C) calcified *Lyngbya*-type cyanobacteria (CLT) and framboids of pyrite (FPy) of subspherical shape filling open spaces between calcified cyanobacteria. (D) Detailed view of octahedral pyrite crystals (OPy) and aragonite needle-shaped crystals (AC). (E) curved cluster of minute pyrite crystals (CCPy) formed on calcite crystals (CC); note the size difference to the octahedral pyrite (OPy) observed on the left-side of the cluster. (F) Detailed view of framboidal pyrite on aragonite needle-shaped crystals (AC); note the size difference between the framboidal forms (FPy) and octahedral pyrite (OPy) observed at the top. Instrument: Nova Nano SEM230 (FEG-SEM) (CAT-URJC).

example, carbonate is present as globules in the melilitite glass and as inclusions within large clinopyroxene and olivine grains at the CVF (Bailey *et al.* 2005). Besides, Humphreys *et al.* (2010) found an inclusion of aragonite in an olivine crystal from a leucitite lava flow from the CVF, which provides evidence for high-pressure crystallization and carbonatitic activity beneath the geophysical lithosphere (>100 km at CO_2-H_2O-bearing mantle solidus temperatures). This, together with the presence of carbonatites at the CVF (Stoppa *et al.* 2012), provides solid,

almost undisputable evidence for a deep-seated (mantle) origin of CO_2. Furthermore, as recently indicated by Bailey and Kearns (2012), all the intra-continental basaltic vents examined in Spain and France to date have erupted carbonatite magma. In this regard, there is a reason for such consistency, because as shown by Holloway (1998), the solubility of CO_2 in magmas is strongly dependent on melt composition, that is, it has low solubility in silica-rich melts and high solubility in silica-poor melts rich in alkalies.

Thus, the presence of alkaline basaltic rocks in the vicinity of Mazarrón (Cebriá *et al.* 2009), coupled to regional geophysical evidence for ascending magma diapirs (Julià *et al.* 2005), suggests some few things. On the one side, the El Saladillo and other CO_2-rich geothermal sites in the Miocene–Pliocene basins of SE Spain are indicative of mantle degasification phenomena at a very large scale. This degasification has been triggered by the generation of CO_2-rich alkaline basaltic magmas that began their ascent and emplacement in Pliocene and Quaternary time. As shown by the very young volcanic activity at Calatrava and Garrotxa (Bailey and Kearns 2012; Puiguriguer *et al.* 2012) (Figure 1(A)), the process is still active. In this respect, we see no reason to discard present magma emplacement at lower or mid-crustal levels beneath the Miocene–Pliocene basins of SE Spain. Moreover, the geothermal activity coupled to the isotopic evidence for carbon (e.g. Cerón *et al.* 2000a) reinforces this scenario. However, CO_2 and the hydrothermal waters may have different origins, and in fact, a typical feature of shallow-seated epithermal ore deposits relates to the key role of meteoric waters. Thus, having magmatic-derived CO_2 does not necessarily imply that the rest of the fluids must have this origin, and in the case of El Saladillo this seems very unlikely as the geochemical modelling suggests. Taking into account the Na–Mg–K relationships (Figure 4(A)), the thermal waters of the El Saladillo can be regarded as 'immature waters' (e.g. Giggenbach 1988), that is, groundwaters with low residence time in the geothermal system or, alternatively, with low or no participation of waters from a deep thermal water reservoir. Given that water–rock interactions do not attain equilibrium, this precludes the application of cation geothermometry. Regarding the major anions, the water composition of the El Saladillo plots in the field of 'sulphate/steam heated waters' (e.g. Giggenbach 1988) (Figure 4(B)). However, as shown by sulphur isotopic data (Pérez del Villar Guillén *et al.* 2008), provenance of sulphate in the El Saladillo groundwater is probably related to the washing of gypsum in upper Miocene evaporite units occurring in the recharge areas at the regional scale (Guadalentín Corridor) (Playá *et al.* 2000) rather than to deep exolved H_2S-rich vapour. Besides, the input of dissolved sedimentary sulphate displaces the anion composition of the water from the HCO_3^- field (Figure 4(B)).

As noted by Pirajno (2007), there is an important link between hydrothermal ore deposits, intraplate volcanism, and mantle plumes, with numerous examples in Australia and Africa. However, in Spain and elsewhere in Europe, this link is missing. Thus, we should first address one question: What makes the Spanish intraplate volcanism different? To start with there is not 'a proper mantle plume' feeding the alkaline basaltic volcanism, but localized diapiric instabilities within the upper asthenosphere (López-Ruiz *et al.* 1993), or as explained by Cebriá *et al.* (2009) for the neighbouring volcanism of Cabezo Negro–La Magdalena (Figure 1(A)), a scenario characterized by the interaction between primitive melts generated from a sublithospheric mantle source and liquids derived from the overlying lithospheric mantle. This accounts for SE Spain or Calatrava, which can be defined as perfect examples of low-volume-type magmatism. If this is the case as it appears to be, then we are not dealing with large- but with very small-scale magmatic events, which may have had important regional consequences for metallogenic activity. Besides, different to the long-lasting activity of large plume heads impacting on the lithosphere (e.g. Campbell and Griffiths 1990; Griffiths and Campbell 1990; Davies and Richard 1992), in Spain we are dealing with time- and

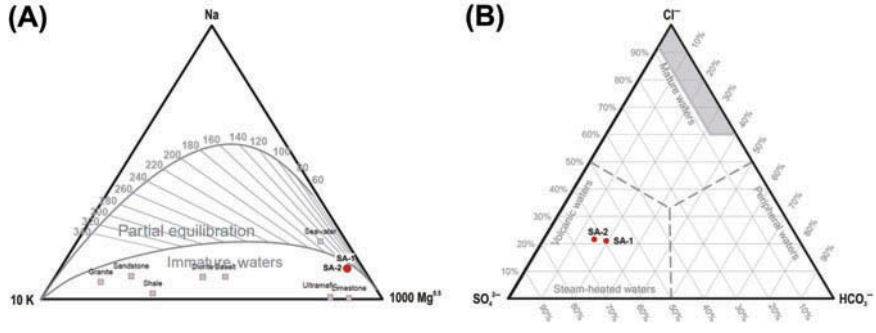

Figure 4. Geothermal modelling for water samples from El Saladillo (based on Giggenbach 1988). (A) Na-10K-1000$Mg^{0.5}$ model, showing the immature character of the groundwater, which precludes the use of geothermometers based on geothermal equilibrium. (B) Cl^-–SO_4^{2-}–HCO_3^- model, showing the sulphate character of the groundwater, far from the field of mature waters.

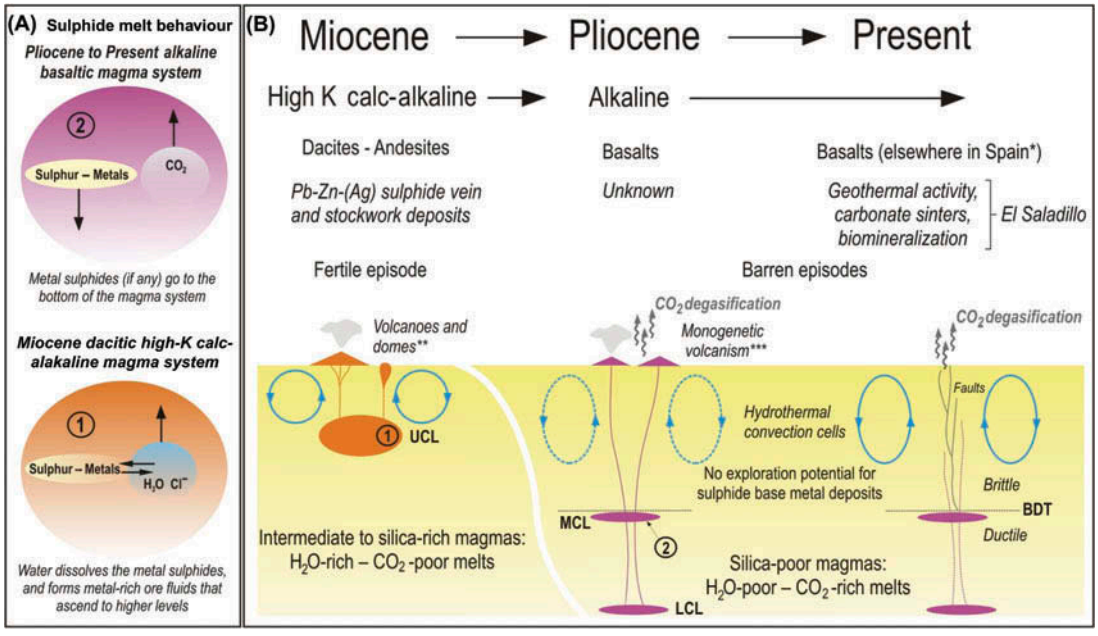

Figure 5. A schematic model (not to scale) for volcanism, CO_2 degasification, and hydrothermal activity at Mazarrón and surrounding areas. (A) Comparison between (high-K) calc–alkaline (1) and alkaline (2) magmatic systems in terms of their potential to scavenge and transport metal sulphides (based on Scaillet 2010). (B) Metallogenic and magmatic evolution from Miocene time onwards, depicting magma chamber emplacement (BDT, brittle-ductile transition; LCL, lower crustal level; MCL, mid-crustal level; UCL, upper crustal level) and hydrothermal convecting cells (LCL and MCL emplacement based on Németh *et al*. 2003); the colours for magma chambers and volcanic landforms are the same used in A (1 and 2). *, Calatrava Volcanic Field, Columbretes Islands, Garrotxa; **, Mazarrón District; ***, La Magdalena–Cabezo Negro (for locations, see Figure 1(A)).

space-limited phenomena, both being negative qualities for the generation of ore deposits.

On the other hand, if the basaltic alkaline volcanism is not S-poor (e.g. Kovalenko *et al.* 2007) where does this sulphur go? One thing is clear, to our knowledge not a single sulphur-base metal economic ore deposit has been formed in the intraplate, European Miocene to Present basaltic alkaline volcanic province, which extends from SE Spain to France (Auvergne) and even Germany (Eiffel) (e.g. Wilson and Downes 2006). In this regard, as shown recently, sulphur follows entirely different paths in calc–alkaline and alkaline magma systems (Nadeau *et al.* 2010; Scaillet 2010) (Figure 5(A)). In alkaline basaltic magmas, a sulphide liquid scavenges ore-forming elements, which settle and accumulate at the bottom of the magma chamber (CO_2 does not interact with other components of the system and escape upwards), whereas in calc–alkaline magmas (which are rich in volatiles) water will dissolve pre-existing sulphides forming metal-rich ore fluids that will move upwards (Scaillet 2010). Besides, the low-volume monogenetic basaltic alkaline volcanism such as that of SE Spain (Cebriá *et al.* 2008) will most probably pond forming small chambers at the upper mantle–continental crust boundary and/or in rheological and density contrast zones between the brittle–ductile transition (BDT) at mid-crustal levels (e.g. Németh *et al.* 2003), that is, far too deep to contribute with metals to shallow-seated hydrothermal systems (Figure 5(B)). Thus, apart from the rather peculiar case of the Almadén Hg ore deposits (Higueras *et al.* 2013), the alkaline magmas will not tend to form base metal sulphide ore deposits at 'upper crustal levels' (Figure 5(B)). We believe that this settles the question of why no sulphide base metal ore deposits have been found in relation to this volcanism in Spain and other sites in Europe; in other words, these volcanic scenarios lack exploration interest for hydrothermal metal sulphides in this European realm.

Last but not least, about 16 years ago Statoil (the Norwegian oil and gas giant) began the injection of carbon dioxide into an aquifer located 800 m beneath the North Sea (Benson and Cole 2008), thus pioneering an idea now popular among earth scientists working on global climate change: CO_2 sequestration in deep sedimentary formations. In this regard, what Statoil did was to reverse what naturally happens in volcanic provinces rich in CO_2. Even if the industrially derived CO_2 emissions could be substantially curbed, which does not seem to be the case unless the totality of the world's financial markets collapses (e.g. Lillo and Oyarzun 2009), the volcanic domains will continue to emit CO_2, in a process that, different to human activities, is unstoppable. We are not implying that the natural emissions of CO_2 are to be regarded *per se* as a global climatic hazard, but nonetheless, they should be considered as an additional and important contributor to the atmospheric

budget of greenhouse gases. After all, it may have been precisely volcanic CO_2 that brought to an end the worst ever planetary glaciation (Snowball Earth episodes), when volcanic degasification substantially raised atmospheric CO_2 in Neoproterozoic time (Hoffman *et al.* 1999).

Conclusions

From a continental perspective, the El Saladillo site might be smaller than the proverbial 'tip of the iceberg', and yet it provides a valuable window for the understanding of much larger scale phenomena, such as the degasification of CO_2 from the mantle via basaltic volcanism and large-scale faults in SE Spain (Figure 5(B)), and at the microscopic scale, the development of microecosystems that drove precipitation of carbonates and sulphides in microbial mats (Figure 3). The El Saladillo site has the typical features of alkaline hot-spring systems, including CO_2-rich waters and carbonate sinter deposits (Figure 2) formed by microbial mats hosting thermophile (*Lingbya* type) cyanobacteria and – most probably – SRB (Figures 3(A)–3(C)). The sinters are base metal poor, a fact related to the meteoric nature of the hydrothermal fluids, but also to the metal-barren character of the deep-seated, intraplate, alkaline, mafic magmatism that triggered this and other young hydrothermal systems in SE Spain. On the one hand, the 'dry' character of these magmas prevents metal extraction by magmatic hydrothermal waters (Figure 5(A)); on the other hand, the deep-seated emplacement of the magmas, at least below the BDT (Németh *et al.* 2003), impede aqueous fluids from reaching this realm (Figure 5(B)). The waters move along fractures; below the BDT, the rocks deform and flow under ductile conditions but do not break. Thus, whatever the case might be, the El Saladillo waters were bound to be metal poor.

El Saladillo offers a clear view of the microscopic world of biomineralization, although as shown earlier, we envisage the interplay of both biotic and abiotic processes (e.g. Rainey and Jones 2009). Given that we took samples with both calcified and living cyanobacterial mats (Figures 2(E) and 3(D)), we were able to observe how these organisms, while keeping the shape, become entirely covered by carbonate, leaving behind enough morphological evidence of the central axial zone once occupied by cyanobacteria (Figure 3(C)). We also noticed the existence of two pyrite mineral phases, one formed by clusters of octahedral crystals of variable sizes (Figures 3(D) and 3(E)) and the other typical framboids composed of minute pyrite crystal at the nanometric scale.

Finally, the area has become relatively popular as a 'cheap spa' among the locals and tourists, who converge there to bathe in the warm waters under no supervision. Moreover, the site is in close proximity to a recreational housing state (Figure 2(A)); thus, given the small size of the site, its fragile nature, and the scientific interest, perhaps the authorities should implement some restrictions to the access.

Acknowledgements

This study was partly supported by Grants CGL2011-23560 and CGL2012-32822 (Ministerio de Economía y Competitividad; Spain). The article benefitted from fruitful conversations on the Pliocene alkaline basaltic volcanism and related CO_2 degasification with Professors Pablo Higueras (UCLM) and Carlos Villaseca (UCM).

References

Alexandratos, V.G., Elzinga, E.J., and Reeder, R.J., 2007, Arsenate uptake by calcite: Macroscopic and spectroscopic characterization of adsorption and incorporation mechanisms: Geochimica et Cosmochimica Acta, v. 71, p. 4172–4187.

APHA, AWWA, WEF, 2005, Standard Methods for the Examination of Water and Wastewater (21st edition): Washington, DC, APHA, AWWA, WEF.

Bailey, K., Garson, M., Kearns, S., and Velasco, A.P., 2005, Carbonate volcanism in Calatrava, central Spain: A report on the initial findings: Mineralogical Magazine, v. 69, p. 907–915.

Bailey, K., and Kearns, S., 2012, New forms of abundant carbonatite – silicate volcanism: Recognition criteria and further target locations: Mineralogical Magazine, v. 76, p. 271–284.

Baumgartner, L.K., Reid, R.P., Dupraz, Ch., Decho, A.W., Buckley, D.H., Spear, J.R., Przekop, K.M., and Visscher, P.T., 2006, Sulfate reducing bacteria in microbial mats: Changing paradigms, new discoveries: Sedimentary Geology, v. 185, p. 131–145.

Benson, S.M., and Cole, D.R., 2008, CO_2 sequestration in deep sedimentary formations: Elements, v. 4, p. 325–331.

Bowell, R.J., 1994, Sorption of arsenic by iron-oxides and oxyhydroxides in soils: Applied Geochemistry, v. 9, p. 279–286.

Butler, I.B., and Rickard, D., 2000, Framboidal pyrite formation via the oxidation of iron (II) monosulfide by hydrogen sulphide: Geochimica et Cosmochimica Acta, v. 64, p. 2665–2672.

Campbell, I.H., and Griffiths, R.W., 1990, Implications of mantle plume structure for the evolution of flood basalts: Earth and Planetary Science Letters, v. 99, p. 79–93.

Cebriá, J.M., López-Ruiz, J., Carmona, J., and Doblas, M., 2008, Quantitative petrogenetic constraints on the Pliocene alkali basaltic volcanism of the SE Spain Volcanic Province: Journal of Volcanology and Geothermal Research, v. 185, p. 172–180.

Cerón, J.C., Pulido-Bosch, A., and Sanz de Galdeano, C., 1998, Isotopic identification of CO_2 from a deep origin in thermomineral waters of southeastern Spain: Chemical Geology, v. 149, p. 251–258.

Cerón, J.C., Martín-Vallejo, M., and García-Rossell, L., 2000a, CO_2-rich thermomineral groundwater in the Betic Cordilleras, southeastern Spain: Genesis and tectonic implications: Hydrogeology Journal, v. 8, p. 209–217.

Cerón, J.C., Jiménez-Espinosa, R., and Pulido-Bosch, A., 2000b, Numerical analysis of hydrogeochemical data: A case study (Alto Guadalentín, Southeast Spain): Applied Geochemistry, v. 15, p. 1053–1067.

Crespo, A., Lunar, R., Oyarzun, R., and Doblas, M., 1995, Unusual case of hot springs-related Co-rich Mn mineralization in central Spain: The Pliocene Calatrava deposits: Economic Geology, v. 90, p. 433–437.

Davies, G.F., and Richard, M.A., 1992, Mantle convection: Journal of Geology, v. 100, p. 151–206.

Doblas, M., and Oyarzun, R., 1989, Neogene extensional collapse in the western Mediterranean (Betic-Rif Alpine orogenic belt): Implications for the genesis of the Gibraltar Arc and magmatic activity: Geology, v. 17, p. 430–433.

Dupraz, Ch., Reid, R.P., Braissant, O., Decho, A.W., Norman, R.S., and Visscher, P.T., 2009, Processes of carbonate precipitation in modern microbial mats: Earth-Science Reviews, v. 96, p. 141–162.

Fouke, B.W., Farmer, J.D., des Marais, D.J., Pratt, L., Sturchio, N.C., Burns, P.C., and Discipulo, M.K., 2000, Depositional facies and aqueous–solid geochemistry of travertine-depositing hot springs (Angel Terrace, Mammoth Hot Springs, Yellowstone National Park, U.S.A.): Journal of Sedimentary Research, v. 70, p. 565–585.

Giggenbach, W.F., 1988, Geothermal solute equilibria: Derivation of Na–K–Mg–Ca geoindicators: Geochimica et Cosmochimica Acta, v. 52, p. 2749–2765.

Griffiths, R.W., and Campbell, I.H., 1990, Stirring and structure in mantle plumes: Earth and Planetary Science Letters, v. 99, p. 66–78.

Higueras, P., Oyarzun, R., Lillo, J., and Morata, D., 2013, Intraplate mafic magmatism, degasification, and deposition of mercury: The giant Almadén mercury deposit (Spain) revisited: Ore Geology Reviews, v. 51, p. 93–102.

Hoffman, P.F., Kaufman, A.J., Halverson, G.P., and Schrag, D.P., 1999, A Neoproterozoic Snowball Earth: Science, v. 281, p. 1342–1346.

Holloway, J.R., 1998, Graphite-melt equilibria during mantle melting: Constraints on CO_2 in MORB magmas and the carbon content of the mantle: Chemical Geology, v. 147, p. 89–97.

Humphreys, E.R., Bailey, K., Hawkesworth, C.J., Wall, F., Najorka, J., and Rankin, A.H., 2010, Aragonite in olivine from Calatrava, Spain – evidence for mantle carbonatite melts from >100 km depth: Geology, v. 38, p. 911–914.

Julià, J., Mancilla, F., and Morales, J., 2005, Seismic signature of intracrustal magmatic intrusions in the Eastern Betics (Internal Zone), SE Iberia: Geophysical Research Letters, v. 32, p. L16304. doi:10.1029/2005GL023274.

Kovalenko, V.I., Naumov, V.B., Girnis, A.V., Dorofeeva, V.A., and Yarmolyuk, V.V., 2007, Average compositions of magmas and mantle sources of mid-ocean ridges and intraplate oceanic and continental settings estimated from the data on melt inclusions and quenched glasses of basalts: Petrology, v. 15, p. 335–368.

Krekeler, D., Teske, A., and Cypionka, H., 1998, Strategies of sulfate-reducing bacteria to escape oxygen stress in a cyanobacterial mat: FEMS Microbiology Ecology, v. 25, p. 89–96.

Lillo, J., and Oyarzun, R., 2009, How short can short-term human-induced climate oscillations be? Science of the Total Environment, v. 407, p. 3605–3608.

Lukavský, J., Furnadzhieva, S., and Pilarski, P., 2011, Cyanobacteria of the thermal spring at Pancharevo, Sofia, Bulgaria: Acta Botanica Croatica, v. 70, p. 191–208.

Nadeau, O., Williams-Jones, A.E., and Stix, J., 2010, Sulphide magma as a source of metals in arc-related magmatic hydrothermal ore fluids: Natural Geoscience, v. 3, p. 501–505.

Németh, K., White, J.D.L., Reay, A., and Martin, U., 2003, Compositional variation during monogenetic volcano growth and its implications for magma supply to continental volcanic fields: Journal of the Geological Society, v. 160, p. 523–530.

Ohfuji, H., and Rickard, D., 2005, Experimental syntheses of framboids – a review: Earth-Science Reviews, v. 71, p. 147–170.

Oyarzun, R., Márquez, A., Ortega, L., Lunar, R., and Oyarzún, J., 1995, A late Miocene metallogenic province in southeast Spain: Atypical Andean-type processes on a smaller scale: Transactions of the Institution of Mining and Metallogy B, v. 104, p. 197–202.

Oyarzun, R., Lillo, J., and Oyarzun, J., 2008, No water, no cyanobacteria – no calc-alkaline magmas: Progressive oxidation of the early oceans may have contributed to modernize island-arc magmatism: International Geology Review, v. 50, p. 885–894.

Oyarzun, R., Lillo, J., López-García, J.A., Esbrí, J.M., Cubas, P., Llanos, W., and Higueras. P., 2011, The Mazarrón Pb-(Ag)-Zn mining district (SE Spain) as a source of heavy metal contamination in a semiarid realm: Geochemical data from mine wastes, soils, and stream sediments: Journal of Geochimical Exploration, v. 109, p. 113–124.

Parkhurst, D.L., and Appelo, C.A.J., 1999, User's guide to PHREEQC (version 2) – A computer program for speciation, batch-reaction, one-dimensional transport, and inverse geochemical calculations: U.S. Geological Survey Water-Resources Investigations Report 99–4259, Denver, 312 p.

Pentecost, A., 1995, Significance of the biomineralizing microniche in a Lyngbya (cyanobacterium) travertine: Geomicrobiology Journal, v. 13, p. 213–222.

Pérez del Villar Guillén, L., Pelayo, M., Prado, A.M., Recreo, F., Vilanova, E., Grandia, F., Duro. L., Doménech, C., Martell, M., Delgado, A., Auqué, L.F., Gimeno, M.J., and Acero, P., 2008, Almacenamiento geológico de CO_2: análogos naturales del almacenamiento y escape; Fundamentos, ejemplos y aplicaciones para la predicción de riesgos y la evaluación del comportamiento a largo plazo. DIGITAL.CSIC. http://digital.csic.es/handle/10261/40531 (accessed 10 February 2013).

Pirajno, F., 2007, Mantle plumes, associated intraplate tectonomagmatic processes and ore systems: Episodes, v. 30, p. 6–19.

Playá, E., Ortí, F., and Rosell, L., 2000, Marine to nonmarine sedimentation in the Upper Miocene evaporites of the Eastern Betics, SE Spain: Sedimentological and geochemical evidence: Sedimentary Geology, v. 133, p. 135–166.

Powell, T., and Cumming, W., 2010, Spreadsheets for geothermal water and Gas Geochemistry: *in* Proceedings of the Thirty-fifth Workshop on Geothermal reservoir engineering: Stanford University, Stanford, California, February 1–3. SGP-TR–188. http://www.geothermal-energy.org/pdf/IGAstandard/SGW/2010/powell.pdf (accessed 10 February 2013).

Puiguriguer, M., Alcalde, G., Bassols, E., Burjachs, F., Expósito, I., Planagumá, L., Saña, M., and Yll, E., 2012, ^{14}C dating of the last Croscat volcano eruption (Garrotxa Region, NE Iberian Peninsula): Geologica Acta, v. 10, p. 43–47.

Rainey, D.K., and Jones, B., 2009, Abiotic versus biotic controls on the development of the Fairmont Hot Springs carbonate deposit, British Columbia, Canada: Sedimentology, v. 56, p. 1832–1857.

Rodríguez, P., and Hidalgo, R., 1997, Valoración de los recursos minerales en el núcleo minero de Mazarrón, *in* Navarro Flores, A., and García-Rosell Martínez, L., eds., Recursos naturales y Medio ambiente en el sureste peninsular: Almería, Instituto de Estudios Almerienses, p. 253–267.

Scaillet, B., 2010, Volatile destruction: Nature, v. 3, p. 456–457.

Smedley, P.L., and Kinniburgh, D.G., 2002, A review of the source, behaviour and distribution of arsenic in natural waters: Applied Geochemistry, v. 17, p. 517–568.

Stoppa, G., Rosatelli, G., Schiazza, M., and Tranquilli, A., 2012, Hydrovolcanic vs magmatic processes in forming maars and associated pyroclasts: The Calatrava -Spain- case history, *in* Stoppa, F., ed., Updates in volcanology – a comprehensive approach to volcanological problems, InTech. doi: 10.5772/25264.

Wargin, A., Olańczuk-Neyman, K., and Skucha, M., 2007, Sulphate-reducing bacteria, their properties and methods of elimination from groundwater: Polish Journal of Environmental Studies, v. 16, p. 639–644.

Wei, D., and Osseo-Asare, K., 1996, Particulate pyrite formation by the Fe^{3+}/HS^{-} reaction in aqueous solutions: Effects of solution composition: Colloids and Surfaces A, v. 118, p. 51–61.

Wilson, M., and Downes, H., 2006, Tertiary-Quaternary intraplate magmatism in Europe and its relationship to mantle dynamics, *in* Gee, D.G., and Stephenson, R., eds., European lithosphere dynamics: London, Geological Society of London Memoir 32, p. 147–166.